ACSNANO

www.acsnano.org

$Ti_3C_2T_x$ MXene Flakes for Optical Control of Neuronal Electrical Activity

Yingqiao Wang, Raghav Garg, Jane E. Hartung, Adam Goad, Dipna A. Patel, Flavia Vitale, Michael S. Gold, Yury Gogotsi, and Tzahi Cohen-Karni*

Cite This: *ACS Nano* 2021, 15, 14662–14671

Read Online

ACCESS | Metrics & More | Article Recommendations | Supporting Information

ABSTRACT: Understanding cellular electrical communications in both health and disease necessitates precise subcellular electrophysiological modulation. Nanomaterial-assisted photothermal stimulation was demonstrated to modulate cellular activity with high spatiotemporal resolution. Ideal candidates for such an application are expected to have high absorbance at the near-infrared window, high photothermal conversion efficiency, and straightforward scale-up of production to allow future translation. Here, we demonstrate two-dimensional $Ti_3C_2T_x$ (MXene) as an outstanding candidate for remote, nongenetic, optical modulation of neuronal electrical activity with high spatiotemporal resolution. $Ti_3C_2T_x$'s photothermal response measured at the single-flake level resulted in local temperature rises of 2.31 ± 0.03 and 3.30 ± 0.02 K for 635 and 808 nm laser pulses (1 ms, 10 mW), respectively. Dorsal root ganglion (DRG) neurons incubated with $Ti_3C_2T_x$ film (25 μg/cm^2) or $Ti_3C_2T_x$ flake dispersion (100 μg/mL) for 6 days did not show a detectable influence on cellular viability, indicating that $Ti_3C_2T_x$ is noncytotoxic. DRG neurons were photothermally stimulated using $Ti_3C_2T_x$ films and flakes with as low as tens of microjoules per pulse incident energy (635 nm, 2 μJ for film, 18 μJ for flake) with subcellular targeting resolution. $Ti_3C_2T_x$'s straightforward and large-scale synthesis allows translation of the reported photothermal stimulation approach in multiple scales, thus presenting a powerful tool for modulating electrophysiology from single-cell to additive manufacturing of engineered tissues.

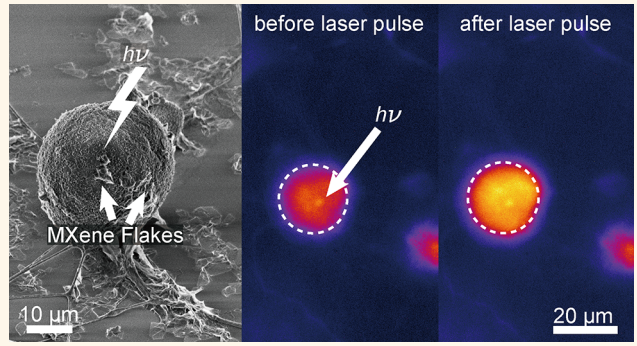

KEYWORDS: *$Ti_3C_2T_x$ MXene, optical, modulation, neurons, dorsal root ganglion*

INTRODUCTION

A key challenge for studying complex neuronal functions is the ability to modulate neuronal activity with high spatiotemporal resolution.[1,2] State-of-the-art microelectrode arrays (MEAs) can stimulate cells with high precision, but they lack cell-type specificity and require invasive implantation, which will result in tissue damage.[3−5] Optogenetics is a major breakthrough that allows remote control without implanted bioelectronics both *in vitro* and *in vivo*, but its requirement for genetic modifications to drive expression of light-sensitive channels limits its clinical translatability.[2,5,6] Alternatively, direct illumination of a neuron's membrane with infrared (IR) laser pulses leads to membrane depolarization, thus resulting in an action potential without implantation or genetic modification.[7,8] However, IR stimulation requires high incident energies per pulse to modulate the cellular activity, which can potentially damage the target cells and tissues.[5,7,8]

Nanomaterial-assisted photothermal stimulation provides a remote, nongenetic approach for stimulating cells and tissues with subcellular spatial (μm) and sub-millisecond temporal resolution.[2,4] Recently, Au- (such as pristine and functionalized Au nanoparticles (AuNPs) and Au nanorods (AuNRs)),[9,10] Si- (mesoporous Si particles, Si nanowires (SiNWs), and Au-decorated SiNWs),[11−13] and C- (carbon nanotubes (CNTs), graphite particles, and nanowire-templated three-dimensional (3D) fuzzy graphene (NT-3DFG))[5,9] based materials were demonstrated as promising candidates for photothermal stimulation without generating cellular stress. However, these materials face at least one of the following challenges: limited near-infrared (NIR) absorbance, low NIR photothermal conversion efficiency, and limited scalability of production.[5,9−13]

Received: May 25, 2021
Accepted: August 10, 2021
Published: August 25, 2021

Transition metal carbides/nitrides (MXenes) have emerged as a rising class of two-dimensional (2D) nanomaterials where atomic layers of transition metals (M) sandwich 2D layer(s) of carbon or nitrogen atoms.[14] Altering the atomic design of MXenes allows the synthesized nanomaterials to exhibit outstanding mechanical properties, high electrical conductivity, excellent electrochemical properties, and tunable optical responses.[14] Therefore, MXenes have found applications across a wide variety of fields such as robotics, photonics, water desalination, and biomedical engineering.[14−20] $Ti_3C_2T_x$[21] have attracted significant attention in photothermal therapy (PTT) due to its high NIR absorbance, high photothermal conversion efficiency, and noncytotoxicity.[19,21−23] Here we demonstrate that $Ti_3C_2T_x$ is an excellent candidate for remote, nongenetic, photothermal stimulation of neuronal electrical activity with high spatiotemporal resolution. Moreover, the synthesis procedure of $Ti_3C_2T_x$ allows large-scale production for establishing biointerfaces across multiple scales.[24,25] $Ti_3C_2T_x$-based photothermal stimulation will provide a powerful toolset for understanding complex neuronal functions and enable optical-based therapeutics for neurological disorders.

RESULTS AND DISCUSSION

2D $Ti_3C_2T_x$ Is a Near-Infrared Absorber. $Ti_3C_2T_x$ flakes were synthesized using a well-established protocol (see Materials and Methods),[26] resulting in 2D flakes with a size of 9.72 ± 1.84 μm^2 and thickness of 2.12 ± 0.41 nm based on atomic force microscopy (AFM) measurements, which suggests the presence of monolayer flakes (Figure 1A and Table S1).[27] $Ti_3C_2T_x$ flakes were confirmed *via* Raman spectroscopy (Figure 1B), where the spectra of individual flakes present four characteristic peaks (Figure 1B, red arrows). A few details can be gleaned from the spectra: the peaks at 147.4 and 200.3 cm^{-1} are attributed to the in-plane and out-of-plane stretching vibrations of Ti atoms, respectively, and the peaks at 640.4 and 723.1 cm^{-1} indicate in-plane and out-of-plane stretching vibrations of C atoms (Figure 1B and Table S2).[28,29] The surface termination of the $Ti_3C_2T_x$ flakes is dominated by −O groups, as indicated by the peak at 385.3 cm^{-1} (Figure 1B, gray region).[28,29] Other terminations include −OH and −F groups, as a result of etching in an aqueous fluorine-containing solution (Figure 1B).

Two-dimensional $Ti_3C_2T_x$ flakes exhibit surface plasmon (SP) resonance where the interband transition to the vacant energy state of the functional groups results in an enhanced absorption in the NIR window.[30,31] Similar optical absorption properties were observed in our $Ti_3C_2T_x$ suspensions (Figure 1C), where the suspensions have an absorption peak at *ca.* 785 nm due to the localized surface plasmon resonance (LSPR) effect (Figure 1C).[30,32,33] The extinction coefficients at 635 and 808 nm were calculated as 19.2 and 21.8 L g^{-1} cm^{-1}, respectively (Figure 1D), which is in good agreement with published data (25.2 L g^{-1} cm^{-1} at 808 nm).[19] Compared with NIR-active absorbers such as AuNRs,[34] and additional absorbers such as SiNWs or NT-3DFG,[5,35] the position of the transverse surface plasmon peak in $Ti_3C_2T_x$ does not depend on the lateral flake size due to the consistency of interband transition and can be tuned by altering the surface chemistry of the material *via* the synthesis protocol.[36,37] The NIR window is crucial for biomedical applications, especially for *in vivo* studies, since the radiation in this window has deeper penetration depths in tissue due to the relatively low absorption by water and hemoglobin.[38] Therefore, $Ti_3C_2T_x$ emerges as a promising candidate for NIR photothermal modulation.

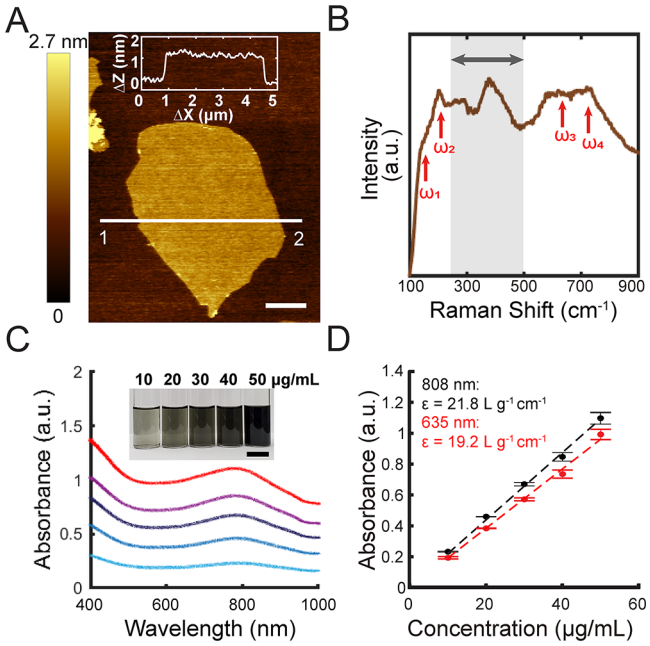

Figure 1. Structural and optical characterization of $Ti_3C_2T_x$. (A) Representative atomic force microscopy (AFM) image of a single-layer $Ti_3C_2T_x$ flake dispersed on a Si/300 nm SiO_2 substrate with an average thickness of 1.16 ± 0.11 nm. Inset: Thickness profile from point 1 to point 2. Scale bar is 1 μm. (B) Representative Raman spectrum of dispersed $Ti_3C_2T_x$ flakes. Red arrows indicate the internal vibration modes of $Ti_3C_2T_x$, and the gray region indicates vibration modes of surface terminations, T_x. (C) Average vis−NIR absorption spectra of $Ti_3C_2T_x$ suspensions of different concentrations (bottom to top: 10, 20, 30, 40, and 50 μg/mL) (n = 3). Inset: Optical image of $Ti_3C_2T_x$ suspensions of different concentrations. Scale bar is 2 cm. (D) Absorbance as a function of $Ti_3C_2T_x$ suspension concentration at 635 nm (red) and 808 nm (black), respectively. Data are presented as mean ± SD (n = 3).

Single-Flake $Ti_3C_2T_x$ Is Photothermally Active. $Ti_3C_2T_x$ exhibits high photothermal conversion efficiency and has been used in PTT for tumor ablation and enhanced water evaporation.[19,22] However, the photothermal performance of $Ti_3C_2T_x$ has only been evaluated at the macroscale using suspensions.[19,22,23] Such measurements do not represent the photothermal effect at a single-flake level due to the interference from the solvent. Precise evaluation of the photothermal effect of $Ti_3C_2T_x$ flakes is necessary prior to stimulating cells and tissues with subcellular precision. Here, we have characterized the photothermal performance of single $Ti_3C_2T_x$ flakes using a micropipette-based technique (Figure 2A, Figure S1) (see Materials and Methods).[5]

The photothermal performance of $Ti_3C_2T_x$ was characterized with both 635 and 808 nm lasers (Figure 2 and Figure S2). For a representative isolated flake (Figure 2B), the local temperature change increased from 0.68 ± 0.02 to 2.31 ± 0.03 K with an increase in the incident laser power from 2 to 10 mW, respectively (635 nm laser, 1 ms pulse, *ca.* 20 μm spot size) (Figure 2C, Figure S2, and Table S3). Illuminating isolated $Ti_3C_2T_x$ flakes with a NIR laser (808 nm, 10 mW, 1 ms pulse, *ca.* 20 μm spot size) resulted in a local temperature change of 3.30 ± 0.02 K (Figure 2D, Figure S2, and Table S4). The greater photothermal performance at 808 nm is attributed

https://doi.org/10.1021/acsnano.1c04431
ACS Nano 2021, 15, 14662−14671

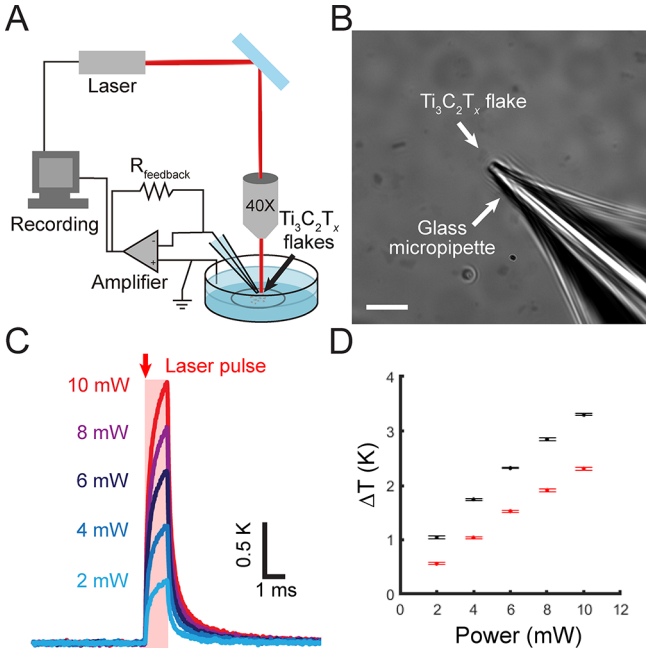

Figure 2. Single $Ti_3C_2T_x$ flake is photothermally active. (A) Schematic of the micropipette-based temperature measurement technique to evaluate the photothermal response of isolated $Ti_3C_2T_x$ flakes. (B) Optical image of an isolated $Ti_3C_2T_x$ flake with a glass micropipette adjacent to the flake. Scale bar is 10 μm. (C) Average temperature change as a function of time for an isolated $Ti_3C_2T_x$ flake (shown in B) under 635 nm laser illumination with a pulse width of 1 ms and different incident laser powers. Data are presented as the average of 10 individual pulses. (D) Maximum temperature change as a function of incident laser power measured for two isolated representative $Ti_3C_2T_x$ flakes under 635 nm (red) and 808 nm (black) laser pulses with a pulse width of 1 ms. Data are presented as mean ± SD for 10 individual laser pulses.

to $Ti_3C_2T_x$'s increased absorption in the NIR window. Our results present that the energy density required by isolated $Ti_3C_2T_x$ flakes to elicit a similar rise in local temperature is at least 1 order of magnitude lower than for AuNRs[39] and AuNPs,[10] 2 orders of magnitude lower than Si-based materials (SiNWs and Au-decorated SiNWs),[12,13] and comparable to recently developed C-based materials (NT-3DFG) (Table S7).[5] Thus, $Ti_3C_2T_x$ is an outstanding photothermally active material at the single-flake level.

To illustrate the ease of implementing $Ti_3C_2T_x$ in photothermal modulation of electrophysiology, we have also evaluated the photothermal response of $Ti_3C_2T_x$ as a film. We prepared $Ti_3C_2T_x$ films by drop-casting known concentrations of $Ti_3C_2T_x$ suspensions onto glass coverslips (Figure S3; see Materials and Methods). The top-view scanning electron microscopy (SEM) images of a 25 μg/cm^2 $Ti_3C_2T_x$ film exhibited a compact morphology, and the cross-section SEM image revealed that the film thickness is 90 ± 35 nm (n = 3 samples, 5 images per sample, 3 measurements per image) (Figure S3). For a representative spot on 25 μg/cm^2 $Ti_3C_2T_x$, the local temperature change was 10.66 ± 0.05 K with the incident laser power of 10 mW (635 nm laser, 1 ms pulse, *ca.* 20 μm spot size). The measured temperature change is *ca.* 5-fold higher compared to individual $Ti_3C_2T_x$ flakes, which is attributed to the accumulating photothermal effect of multiple flakes (Figure S4 and Table S5). Thus, both the photothermally active $Ti_3C_2T_x$ films and flakes can potentially allow photothermal modulation of cellular activity with lower incident energies.

$Ti_3C_2T_x$ Flakes Adhere to the Cell Membrane. Photothermal stimulation of cells leverages on inducing an instantaneous change in the cell membrane capacitance.[9] This requires the photothermally active agent to be in close proximity of the plasma membrane.[9] We investigated the interaction between $Ti_3C_2T_x$ flakes and dorsal root ganglion (DRG) neurons with two types of interfaces: (1) DRG neurons directly cultured on $Ti_3C_2T_x$ films and (2) DRG neurons incubated with dispersed $Ti_3C_2T_x$ flakes. A 25 μg/cm^2 $Ti_3C_2T_x$ film was selected due to its high coverage as well as its semitransparent nature, which allowed transmitted light imaging of the DRG cells using a custom-built microscope (Figure S5). Incubating $Ti_3C_2T_x$ films in physiological conditions did not result in a change of structure and surface terminations, proved by Raman spectra and SEM images before and after incubation. (Figure S6).

Cultured DRG neurons adhered well to the $Ti_3C_2T_x$ film without any delamination (Figure 3A and B). The $Ti_3C_2T_x$ film was observed only below the cultured cells, and no $Ti_3C_2T_x$ flakes were observed inside the cell membrane of the DRG neurons (Figure 3A and B). In the case of dispersed $Ti_3C_2T_x$ flakes on DRG neurons, the flakes were randomly distributed throughout the cell culture and adhered to the cell membrane without any observed internalization after a 24 h incubation period (Figure 3C,D and Figure S7). This close interaction between $Ti_3C_2T_x$ flakes and DRG neurons establishes a promising interface to allow an efficient photothermal stimulation.[9]

Prior to employing $Ti_3C_2T_x$ films and flakes for photothermal stimulation, it is necessary to evaluate their cytotoxicity. To this end, we investigated the cytotoxicity by incubating DRG neurons for up to 6 days with $Ti_3C_2T_x$ films (25 μg/cm^2) and $Ti_3C_2T_x$ flakes (100 μg/mL). The calculated viabilities were 95.4 ± 3.4%, 94.8 ± 3.2%, and 96.5 ± 2.2% for control samples, $Ti_3C_2T_x$ films, and dispersed $Ti_3C_2T_x$ flakes, respectively (Figure 4). The results indicate that $Ti_3C_2T_x$ (as films or flakes) has no detectable influence on neuronal viability (Figure 4).

$Ti_3C_2T_x$ Film Allows Photothermal Stimulation of the DRG Network. To demonstrate the photothermal neuronal modulation capabilities of the $Ti_3C_2T_x$ film, DRG neurons were cultured on a $Ti_3C_2T_x$ film, and neuronal electrical activity during stimulation was evaluated using Ca^{2+} imaging (Figure 5A and Figure S8). Ca^{2+} is a ubiquitous secondary messenger that plays a key role in signal transduction in excitable cells. Therefore, monitoring changes in Ca^{2+} intracellular concentration during an action potential can be used as an indicator to study cellular electrical activity.[5,40] To evaluate the effect of photothermal stimulation on the Ca^{2+} dynamics, DRG neurons were labeled with a Ca^{2+} indicator, CalBryte 520 AM (see Materials and Methods). Ca^{2+} influx was observed after applying a single 1 ms, 10 mW laser pulse (635 nm, 10 μJ (*ca.* 3.2 J/cm^2) per pulse) to the DRG neuron−film interface (Figure 5B, Movie S1). The intracellular Ca^{2+} transient of the laser-targeted neuron (Figure 5B, region of interest 1 (ROI 1)) demonstrated a rapid rise and slow decay, which is in agreement with the reported Ca^{2+} transients for DRG neurons (Figure 5C).[5,35] The $Ti_3C_2T_x$ film-based optical modulation of DRG neurons is highly reproducible (Figure S8, Table S6, and Movie S2). Photothermal stimulation with high-energy laser pulses can potentially lead

https://doi.org/10.1021/acsnano.1c04431
ACS Nano 2021, 15, 14662−14671

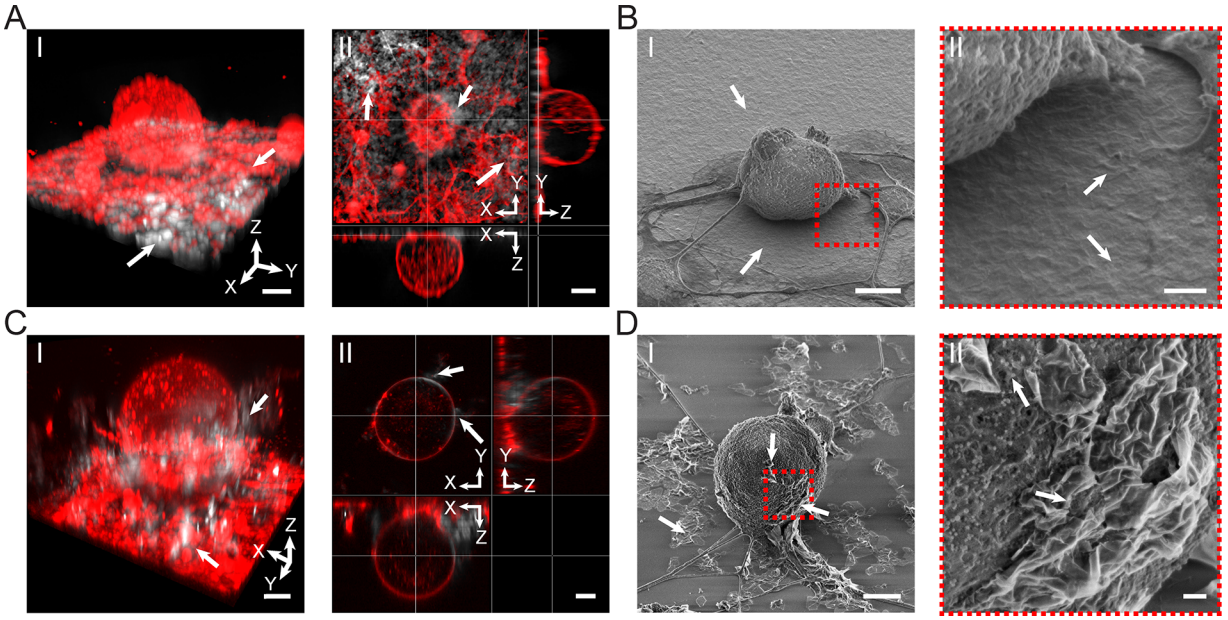

Figure 3. $Ti_3C_2T_x$ interfaces with DRG neurons. (A) Interface between $Ti_3C_2T_x$ films and DRG neurons. (I) Representative 3D reconstructed confocal laser scanning fluorescence image of DRG neurons labeled with plasma membrane stain (red color, CellMask plasma membrane dye) seeded on a 25 μg/cm^2 $Ti_3C_2T_x$ film (white color). The white arrows denote $Ti_3C_2T_x$ flakes. Scale bar is 10 μm. (II) Orthogonal sections of the cell in I. Scale bar is 10 μm. (B) Representative SEM image of DRG neurons seeded on a $Ti_3C_2T_x$ film. Scale bar is 10 μm. (II) Expanded view of the marked red dashed box in I. Scale bar is 1 μm. (C) Interface between dispersed $Ti_3C_2T_x$ flakes and DRG neurons. (I) Representative 3D reconstructed confocal laser scanning fluorescence image of DRG neurons labeled with plasma membrane stain (red color, CellMask plasma membrane dye) incubated for 24 h with a dispersion of 100 μg/mL $Ti_3C_2T_x$ flakes (white color). The white arrows denote $Ti_3C_2T_x$ flakes attached to the neuron. Scale bar is 10 μm. (II) Orthogonal sections of the cell in I. Scale bar is 10 μm. (D) Representative SEM image of a DRG neuron incubated with 100 μg/mL $Ti_3C_2T_x$ flakes. White arrows denote $Ti_3C_2T_x$ flakes interfaced with the neuron and dispersed on the substrate. Scale bar is 10 μm. (II) Expanded view of the marked red dashed box in I. Scale bar is 1 μm.

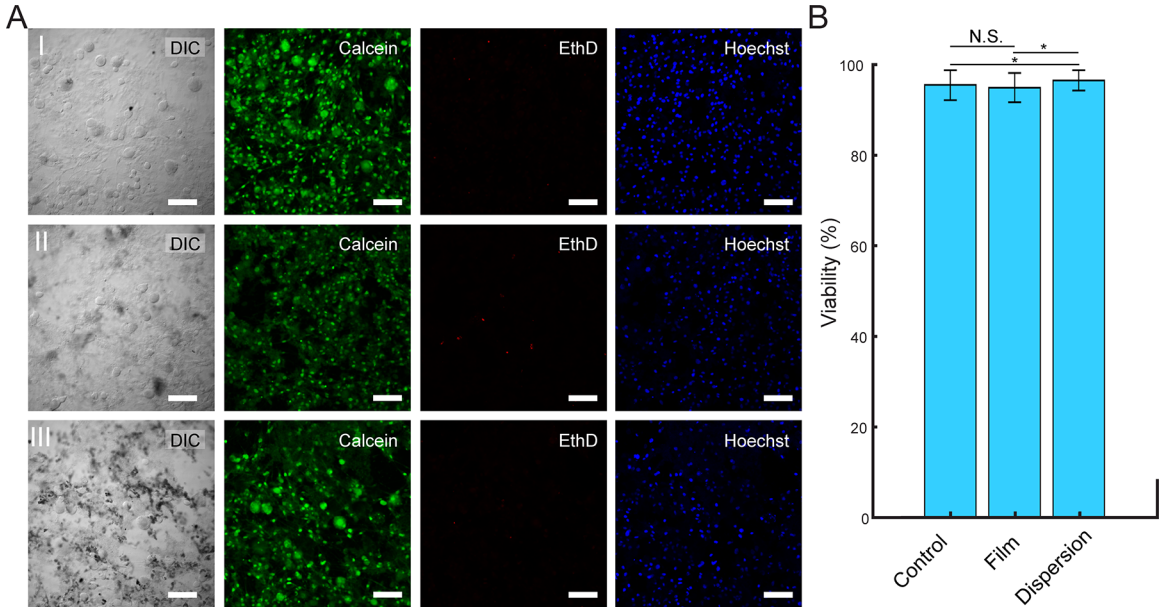

Figure 4. $Ti_3C_2T_x$ films and dispersions do not have detectable influence on DRG neuron viability. (A) Live/Dead assay performed on DRG neurons incubated (I) without $Ti_3C_2T_x$, (II) with 25 μg/cm^2 $Ti_3C_2T_x$ film, and (III) with a 100 μg/mL dispersion of $Ti_3C_2T_x$ flakes for 6 days. Green (Calcien AM), red (ethidium homodimer-1), and blue (Hoechst) denote live cells, dead cells, and cell nuclei, respectively. Scale bars are 100 μm. (B) Viability (%) of DRG neurons incubated without $Ti_3C_2T_x$ (control), on a 25 μg/cm^2 $Ti_3C_2T_x$ film (film), and with a 100 μg/mL dispersion of $Ti_3C_2T_x$ flakes (dispersion). Data are presented as mean ± SD (n = 5 dishes per condition, 10 images per dish). N.S. denotes no significant difference. The asterisks (*) denote statistically significant difference with $p < 0.05$ (one-way ANOVA and *post hoc* Tukey).

to cellular phototoxicity due to the high local temperature change at the cell−material interface.[5] Therefore, it is necessary to minimize the local temperature change required for safe photothermal stimulation by optimizing the overall

https://doi.org/10.1021/acsnano.1c04431
ACS Nano 2021, 15, 14662−14671

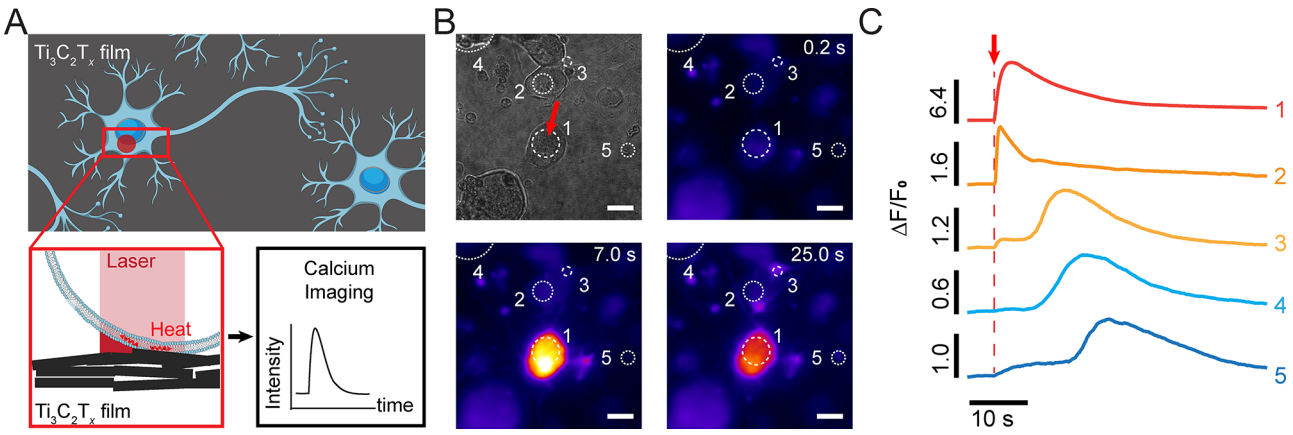

Figure 5. DRG electrical activity can be modulated by the $Ti_3C_2T_x$ film. (A) Schematic representing a photothermal stimulation event at the interface between DRG neurons and the $Ti_3C_2T_x$ film. (B) Bright field and time series fluorescence images of a representative DRG neuron interfaced with a $Ti_3C_2T_x$ film and labeled with a Ca^{2+} indicator (CalBryte 520 AM). A 635 nm laser pulse of 10 mW power and 1 ms pulse duration was applied at t = 5.6 s. Red arrow indicates the laser target spot. The white circles denote the ROIs for fluorescence intensity analysis. Scale bars are 20 μm. (C) Normalized Ca^{2+} fluorescence intensity as a function of time for the ROIs marked in B. Red arrow denotes the starting point of the applied laser pulse (t = 5.6 s).

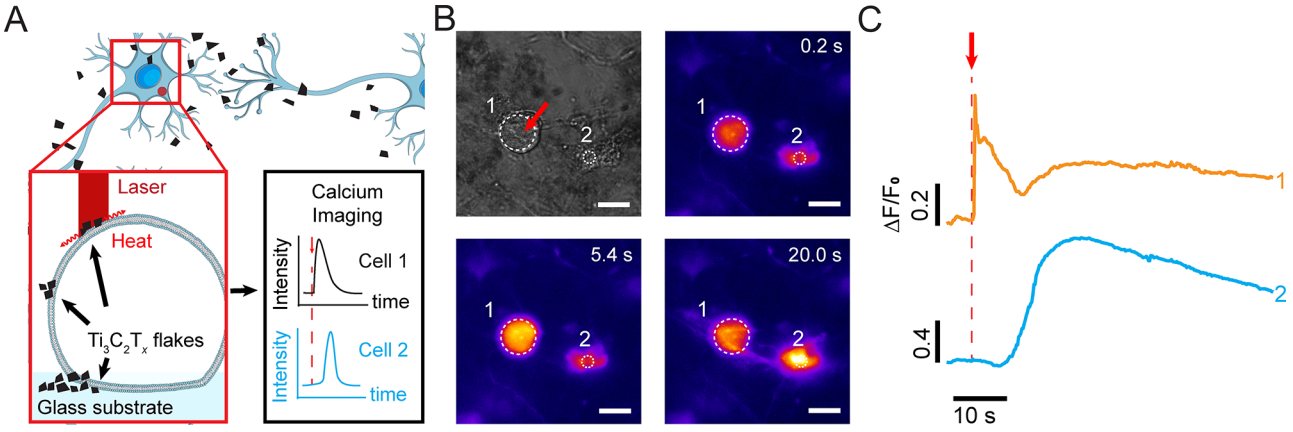

Figure 6. Optical modulation of DRG activity with dispersed $Ti_3C_2T_x$ flakes. (A) Schematic of DRG neuron network and dispersed $Ti_3C_2T_x$ flake interface. (B) Bright field image and time series fluorescence images of a representative DRG neuron labeled with a Ca^{2+} indicator (CalBryte 520 AM). A 635 nm laser pulse of 18 mW power and 1 ms pulse duration was applied at t = 5.0 s. Red arrow indicates the laser target spot. The white circles denote the ROIs for fluorescence intensity analysis. Scale bars are 20 μm. (C) Normalized Ca^{2+} fluorescence intensity as a function of time for the ROIs marked in B. Red arrow denotes the starting point of the applied laser pulse (t = 5.0 s).

energy of the incident laser pulse.[5] We observed that laser energies as low as 2 μJ (*ca.* 0.6 J/cm^2) incident at the DRG–$Ti_3C_2T_x$ interface can successfully stimulate DRG neurons (Table S6). Stimulation of the targeted DRG neuron resulted in delayed Ca^{2+} transients in neighboring cells (Figure 5B and C, ROI 2–5, and Movie S1). The propagation of the Ca^{2+} wave in the network is attributed to the presence of gap junctions and extracellular diffusion of agonists between the cells.[41−43] The exact communication mechanisms between the cells need further investigations.

As reported previously, photothermal stimulation with Si-, Au-, and C- based materials follows the opto-capacitive mechanism.[5,9,35,44] The opto-capacitive mechanism dictates that the light-induced temperature gradient (dT/dt) close to the cell membrane will result in a change in the membrane capacitance, followed by the generation of a transient capacitive current, I_c.[9] Thus, targeting the laser pulse away from the cell–film interface will not generate sufficient I_c to elicit an action potential. To illustrate this point, illuminating the $Ti_3C_2T_x$ film at a point away from a DRG neuron with the same laser pulse conditions did not result in any change in Ca^{2+} fluorescence intensity (Figure S9). This corroborates that the photothermal stimulation with the $Ti_3C_2T_x$ film requires a close interface between the film and the target DRG neurons.

DRG–$Ti_3C_2T_x$ Flake Interface Allows High-Resolution Neuronal Modulation. To achieve optical stimulation with subcellular resolution without coating the entire substrate with $Ti_3C_2T_x$, isolated $Ti_3C_2T_x$ flakes were interfaced with DRG neurons (Figure 6A). A single laser pulse (635 nm, 18 mW, and 1 ms pulse, 18 μJ (ca. 5.7 J/cm^2) per pulse) at the DRG neuron and $Ti_3C_2T_x$ flake interface resulted in an elicit action potential as can be seen in the apparent intracellular Ca^{2+} transient (Figure 6B and C, Movie S3, and Table S6). We note that the energy needed per pulse to stimulate a DRG neuron is higher for dispersed flakes as compared to films due to the higher flake density of the $Ti_3C_2T_x$ film, which results in a higher local temperature change (Figure S4 and Table S5). Targeting the laser at a point on the DRG neuron but not on the $Ti_3C_2T_x$ flake did not result in any Ca^{2+} transients (off-$Ti_3C_2T_x$, Figure S10). Additionally, targeting the laser at a

https://doi.org/10.1021/acsnano.1c04431
ACS Nano 2021, 15, 14662−14671

point away from the DRG neurons did not result in any Ca^{2+} transients as well (off-cell, Figure S10). These results indicate that isolated $Ti_3C_2T_x$ flakes allow effective optical modulation with subcellular spatial resolution.

CONCLUSIONS

In this work, we demonstrate that 2D $Ti_3C_2T_x$ (MXene) can be used for remote and nongenetic modulation of neuronal electrical activity with subcellular resolution. We have measured the $Ti_3C_2T_x$ photothermal performance at the single-flake level and observed a local temperature change of 2.31 ± 0.03 and 3.30 ± 0.02 K under 635 and 808 nm pulses (10 mW and 1 ms), respectively. $Ti_3C_2T_x$ flakes interfaced with DRG neurons do not alter cellular viability and are not internalized; instead they adhere closely to the cell membrane. Both $Ti_3C_2T_x$ films and flakes enabled photothermal stimulation of DRG neurons with microjoule-scale energies per laser pulse (2 μJ (*ca.* 0.6 J/cm^2) for film and 18 μJ (*ca.* 5.7 J/cm^2) for flakes). The effective energy densities for photothermal stimulation with $Ti_3C_2T_x$ are at least 1 order of magnitude lower than those for existing Au-[9,10] and Si-[11−13] based photothermal agents and comparable to C-based materials (NT-3DFG) (Table S8).[5] Compared with a photoelectrically active p−i−n Si membrane and SiNWs,[12,45] $Ti_3C_2T_x$ necessities similar incident energy densities to stimulate neurons. Besides the low incident energy densities, $Ti_3C_2T_x$ will allow translation of the reported photothermal stimulation approach in future biomedical engineering applications and interventions with the ease of straightforward and large-scale synthesis.[24] Furthermore, this technique can be potentially combined with electrical stimulation and employed in tissue engineering for building the prototype of practical therapeutics.[46−48]

MATERIALS AND METHODS

Synthesis of $Ti_3C_2T_x$. $Ti_3C_2T_x$ synthesis follows a previously published protocol.[26] TiC (99.5%, ∼325 mesh, Alfa Aesar, catalog no. 40178-30), Ti (99.5%, ∼325 mesh, Alfa Aesar, catalog no. 42624-22), and Al (99.5%, ∼325 mesh, Alfa Aesar, catalog no. 11067-30) powders in a 2:1:1 mass ratio were mixed with zirconia balls at a 2:1 zirconia-to-powder ratio in a ball mill at 70 rpm for 18 h. The mixed powder was placed in an alumina crucible, covered by graphite foil, and placed into a tube furnace. The tube furnace was purged with a 100 sccm Ar flow for 30 min at room temperature followed by heating to 1380 °C for 2 h at a heating/cooling rate of 3 °C/min. The Ti_3AlC_2 block was milled to form a Ti_3AlC_2 powder using a TiN-coated milling bit. One gram of Ti_3AlC_2 powder was then slowly mixed with 10 mL of 9 M HCl (Fisher Scientific, catalog no. 320331) and stirred for 4 h at room temperature. The mixture was vacuum filtered with a 5 μm filter membrane, and the residual powder was washed with DI-H_2O until the pH of the filtrate was *ca.* 6. The washed Ti_3AlC_2 powder was dried in a vacuum oven for 6 h at 80 °C and was collected after sieving through a 450-mesh (32 μm) particle sieve. A 6 mL amount of DI-H_2O, 12 mL of 12 M HCl, and 2 mL of 50 wt % HF (Acros Organics, catalog no. AC223330250) were added in a 60 mL high-density polyethylene bottle. A 1 g portion of Ti_3AlC_2 power was added to the prepared solution and mixed at 400 rpm for 24 h at 35 °C.

The mixture was centrifuged in a 175 mL centrifuge tube at 3500 rpm for 5 min, followed by decantation and redispersing the sediment with DI-H_2O. This process was repeated until the supernatant reached a pH of *ca.* 6 to obtain a multilayer $Ti_3C_2T_x$ sediment. The sediment was dispersed into 50 mL of a 0.5 M LiCl solution (99.3% Chem-Impex Int. catalog no. 30595) and stirred at 400 rpm for 4 h at room temperature. The sediment was washed with DI-H_2O and centrifuged at 3500 rpm for 5 min. The supernatant was decanted, and the sediment was redispersed in DI-H_2O and centrifuged at 3500 rpm for 1 h. This step was repeated three more times. Finally, the $Ti_3C_2T_x$ suspension was centrifuged at 3500 rpm for 20 min and the supernatant was collected.

Atomic Force Microscopy (AFM). AFM was performed using a MultiMode 8-HR (Bruker) in tapping mode. A 0.5 mg/mL $Ti_3C_2T_x$ suspension was spin-coated at 2000 rpm for 2 min on an O_2-plasma-treated Si/300 nm SiO_2 substrate, followed by spinning at 5000 rpm for 15 s to dry the sample. A Si tip (Budget Sensors, USA, Tap300Al-G; f_0 = 300 kHz, k = 40 N/m) was used to characterize the samples. Scan speed was 0.8 Hz.

Raman Spectroscopy. Raman spectra of isolated $Ti_3C_2T_x$ flakes were acquired using NT-MDT Spectra (NT-MDT Spectrum Instruments) with a 532 nm excitation laser using a 100×/0.7 NA objective. To prepare the sample, 20 μL of a 10 μg/mL $Ti_3C_2T_x$ suspension was drop-casted on a Si/600 nm SiO_2 substrate coated with 100 nm Au. The spectra were acquired with a 0.5 neutral density filter and a 30 s acquisition time. The measured laser power through the objective was 1.95 mW (PM100D power meter equipped with a S121C detector, Thorlabs). The spectra were acquired from 10 randomly distributed points across 3 independent samples.

Visible−Near Infrared (Vis-NIR) Absorption Spectroscopy. Vis−NIR absorption spectroscopy was characterized using an ASEQ LR1-T broad range photospectrometer (ASEQ Instruments). Vis−NIR absorption spectra were acquired from five different concentrations of $Ti_3C_2T_x$ suspensions (10, 20, 30, 40, and 50 μg/mL). Three independent spectra were measured for each concentration, and the results are presented as the mean of these three independent measurements. The extinction coefficient was determined following the Beer−Lambert law:[49]

$$A = \varepsilon L c$$

where A is the absorbance, ε is the extinction coefficient, L is the length of the cuvette (1 cm), and c is the concentration of $Ti_3C_2T_X$ suspensions. Linear curve fitting was performed using MATLAB (MathWorks) to calculate the extinction coefficients.

Scanning Electron Microscopy (SEM). SEM imaging was performed using a FEI Quanta 600 field emission gun SEM. Images were acquired with an acceleration voltage of 2−20 kV and 5 mm working distance. No additional conductive coating was applied to any of the samples for SEM imaging.

$Ti_3C_2T_x$ Film Preparation. $Ti_3C_2T_x$ films of different densities were prepared on 0.9 cm × 0.9 cm microscope cover glass (Fisher Scientific, catalog no. 12-541A). The substrates were cleaned in an ultrasonic bath (Crest Ultrasonics, model no. CP230D) in acetone for 5 min, followed by isopropyl alcohol washing and N_2 blow drying. The surfaces were coated with poly-L-lysine (PLL) (Sigma-Aldrich, catalog no. P8920). $Ti_3C_2T_x$ suspensions (50 μL) of different concentrations were drop-casted and air-dried at room temperature to obtain 15, 25, 35, 45, and 55 μg/cm^2 $Ti_3C_2T_x$ films.

Photothermal Characterization. Photothermal characterization of isolated $Ti_3C_2T_x$ flakes was performed using a previously described micropipette technique with a custom-built microscope.[5] 635 or 808 nm laser (NaKu Technology) pulses were delivered using a custom-built microscope with a 40×/0.80 NA water immersion objective (Nikon). The duration of the laser pulses was controlled using a transistor−transistor logic (TTL) signal. Prior to the photothermal characterization, the output power of the laser through the objective was calibrated under continuous wave operation using a photodiode power meter (PM100D with an S121C detector, Thorlabs).

Voltage-clamp measurement was performed using a patch-clamp amplifier (A-M Systems model 2400) controlled by WinWCP software (open-source). Micropipettes were pulled from glass capillaries with a 1.5 mm outer diameter and 0.86 mm inner diameter (Sutter Instruments, catalog no. BF150-86-10) using a micropipette puller (P-97, Sutter Instruments) for a final resistance of *ca.* 1−2 MΩ in 1× phosphate buffered saline (1× PBS) solution (Corning, catalog no. 21-040-CV). For photothermal characterization, $Ti_3C_2T_x$ flakes were dispersed on a PLL-modified glass-bottom dish (Matsunami, catalog no. D35-14-1.5-U). Briefly, the dish was treated under UV-

https://doi.org/10.1021/acsnano.1c04431
ACS Nano 2021, 15, 14662−14671

Ozoneat 25 °C for 10 min followed by addition of 100 μL of 0.02% (w/v) PLL for 5 min. The PLL solution was aspirated, and the dish was washed three times with DI-H_2O and N_2 blow-dried. Twenty microliters of a 10 μg/mL $Ti_3C_2T_x$ suspension was drop-casted on the surface-treated dish and air-dried at room temperature. During the photothermal characterization, the dish was filled with 4 mL of 1× PBS solution and a Ag/AgCl wire was placed in the chamber. The temperature of the solution was continuously measured using a digital thermometer (Signstek, 6802-II). The isolated $Ti_3C_2T_x$ flake was selected through the microscope, and the glass micropipette tip was controlled by a manipulator to get approximately 1−2 μm from the selected flake to record the local temperature change. The tip was located at the edge of the flake to avoid the light reflected by the pipette walls. The current through the micropipette and the resistance of the micropipette were continuously recorded in voltage-clamp mode with holding potential V_p of 75 mV. One millisecond laser pulses with power ranging from 2 to 10 mW were applied. The photothermal current ($\Delta I_{thermal}(t)$) can be expressed using the following equation:[5]

$$\Delta I_{thermal}(t) = \left(\frac{R_0}{R(t)} - 1\right) \times I_0 \quad (1)$$

where $\Delta I_{thermal}(t)$, R_0, $R(t)$, and I_0 are the photothermal current, the micropipette resistance at room temperature, the micropipette resistance during laser illumination, and the dark-state current, respectively. To calibrate the resistance of the micropipette as a function of temperature, 4 mL of 1× PBS solution was heated to *ca.* 50 °C and added into a Petri dish. A thermocouple was placed near the micropipette's tip to measure the temperature. To establish a calibration curve, the micropipette's resistance was recorded until a bath temperature of 25 °C was reached (Figure S1). The dependence between the micropipette's resistance and temperature follows the Arrhenius law:[50]

$$\ln\left(\frac{R(t)}{R_0}\right) = \frac{A}{T} + C \quad (2)$$

where $R(t)$, R_0, A, T, and C are the measured micropipette resistance, the room-temperature micropipette resistance, the calibration curve slope, the temperature, and the calibration curve intercept, respectively. Photothermal characterization of 7 and 10 independent $Ti_3C_2T_x$ flakes was performed with 635 and 808 nm lasers, respectively. Photothermal characterization of $Ti_3C_2T_x$ films (25 μg/cm^2) was performed under 635 nm laser illumination at 10 randomly selected spots across two representative film samples.

Dorsal Root Ganglion (DRG) Cell Culture. DRG neurons were obtained from adult male Sprague−Dawley rats (Envigo) and were harvested as described previously.[5,42] Rats with weights between 240 and 400 g were pair-housed with a 12:12 light:dark cycle with food and water *ad libitum*, at the University of Pittsburgh. The experiments were approved by the University of Pittsburgh Institutional Animal Care and Use Committee and followed NIH guidelines for laboratory animal use. Prior to harvesting DRG neurons, rats were anesthetized with an intraperitoneal injection of a mixture containing 55 mg/kg ketamine (Henry Schein, catalog no. 056344), 5.5 mg/kg xylazine (Henry Schein, catalog no. 033197), and 1.1 mg/kg aceprozamine (Henry Schein, catalog no. 003845). Rats were subsequently perfused with 1× PBS, and DRG neurons were collected, enzymatically treated, and mechanically dissociated to prepare cell seeding suspensions.

DRG neurons were then seeded on uncoated and $Ti_3C_2T_x$ film coated glass-bottom dishes. Briefly, dishes were treated with UV-Ozone at 25 °C for 10 min and sterilized with 70% ethanol (Pharmco-Aaper, catalog no. 111000200) and UV illumination for 1 h. The dishes were then rinsed three times with sterile DI-H_2O, treated with 300 μL of 50 μg/mL poly-D-lysine (PDL) (Sigma-Aldrich, catalog no. P6407) at room temperature for 1 h, rinsed three times with sterile DI-H_2O, and dried for 30 min in a cell culture hood under sterile conditions. The PDL-coated dishes were incubated with 250 μL of 20 μg/mL Laminin (Corning, catalog no. 354232) at 37 °C with 5% CO_2 for 1 h and subsequently rinsed three times with sterile 1× PBS. DRG neurons were seeded on the PDL-laminin-treated dishes and incubated at 37 °C with 5% CO_2 for 3 h prior to adding 4 mL of media. The media was composed of Dulbecco's modified Eagle's medium (Corning, catalog no. 15-013-CM) + 1% Glutamax (ThermoFisher, catalog no. 35050-061) + 1% penicillin/streptomycin (ThermoFisher, catalog no. 15140122) + 10% fetal bovine serum (Invitrogen, catalog no. 10082147). The DRG neurons were incubated at 37 °C with 5% CO_2 for 24−48 h until use.

Interfacing DRG Neurons with $Ti_3C_2T_x$. To investigate the DRG-$Ti_3C_2T_x$ interfaces, DRG neurons were interfaced with $Ti_3C_2T_x$ films and flakes. DRG−film interfaces followed the sample preparation protocol described above. To interface DRG neurons and dispersed $Ti_3C_2T_x$ flakes, a $Ti_3C_2T_x$ suspension was sterilized under UV illumination for 1 h and added to the DRG neuron culture with a final concentration of 100 μg/mL. The dishes with dispersed flakes were incubated at 37 °C with 5% CO_2 for 24 h. CellMask orange plasma membrane stain (ThermoFisher, catalog no. C10045) was used to stain the cell membrane. The cell cultures were incubated with dye (5 μg/mL) for 15 min at 37 °C with 5% CO_2. Tyrode's buffer solution (Sigma, catalog no. T2145) with a pH of *ca.* 7.4 supplemented with 1 g/L $NaHCO_3$ (Sigma, catalog no. S576) was constantly perfused with carbogen gas containing 5% CO_2 and 95% O_2 (Airgas) for 20 min. The samples were gently washed three times with carbogenated Tyrode's solution. The DRG neuron and $Ti_3C_2T_x$ interface was imaged using *z*-stack live-cell imaging with differential interference contrast (DIC) and scanning laser confocal fluorescence imaging with a 40×/0.80 NA water immersion objective. The 3D reconstructions and orthogonal sections were generated using Imaris 3/4D Image Visualization and Analysis software (Oxford Instruments).

The samples were then fixed using 4% paraformaldehyde (Electron Microscopy Sciences, catalog no. 15710) in 1× PBS for 20 min on a plate shaker at room temperature. The samples were rinsed three times with 1× PBS, followed by washing three times with DI-H_2O. DI-H_2O was serially replaced with 100% ethanol (25%, 50%, 75%, 90%, and 100%). During each exchange, the samples were incubated at room temperature for 10 min. The 100% ethanol was serially exchanged with hexamethyldisilazane (HMDS) (Sigma-Aldrich, catalog no. 440191) (50% and 100%) and incubated at room temperature for 20 min during each exchange. HMDS was then aspirated, and the samples were dried in a clean hood at room temperature. Fixed and dried samples were imaged using SEM without any additional surface coatings with an acceleration voltage and working distance of 2 kV and 5 mm, respectively.

Viability Assay. Viability analysis was performed on DRG neurons seeded on glass-bottom dishes (control), seeded on 25 μg/cm^2 $Ti_3C_2T_x$ films (film), and incubated with a 100 μg/mL dispersion of $Ti_3C_2T_x$ flakes (dispersion). The samples were prepared following the above sample preparation protocols. For all samples, the seeding density of DRG neurons was 4500 cells/dish. To maintain neuronal phenotypes, culture media was supplemented with 10 nM/mL 2.5S NGF (Sigma-Aldrich, catalog no. 01-125). To minimize the proliferation of glial cells, mitotic inhibitors uridine (Sigma-Aldrich, catalog no. 3750) and deoxyuridine (Sigma-Aldrich, catalog no. D5412) were added to the culture media at a final concentration of 40 μM. The samples were maintained in culture at 37 °C with 5% CO_2 for 6 days before performing the viability assay. For the assay, the samples were labeled with a Live/Dead assay kit (ThermoFisher, catalog no. L3224). The live cells were labeled with 2 μM calcein acetoxymethyl (Calcein AM); the dead cells were labeled with 4 μM ethidium homodimer-1 (EthD-1); and the nuclei were labeled with 1 μM Hoechst 33342 (ThermoFisher, catalog no. 62249). After adding the dyes, the samples were incubated for 15 min at 37 °C with 5% CO_2. The samples were then washed three times with warm carbogenated Tyrode's solution. DIC and scanning laser confocal fluorescence imaging were performed using an upright confocal microscope and a 20×/0.50 NA water immersion objective (Nikon). Viability quantification was performed for 5 dishes per condition and 10 images per dish. The viability was calculated as

https://doi.org/10.1021/acsnano.1c04431
ACS Nano 2021, 15, 14662−14671

$$\text{Viability (\%)} = \frac{\text{Total no. of cells} - \text{No. of dead cells}}{\text{Total no. of cells}} \times 100$$

Ca^{2+} Imaging of Photothermal Stimulation. To Ca^{2+} image the neurons during photothermal stimulation, DRG neurons interfaced with $Ti_3C_2T_x$ films and dispersed $Ti_3C_2T_x$ flakes were labeled with a Ca^{2+} indicator dye by incubating the samples with 5 μM CalBryte-520 (AAT Bioquest, catalog no. 20650) for 60 min at 37 °C followed by 30 min at room temperature in the dark. The samples were then washed three times with carbogenated Tyrode's solution and were loaded on the stage of the custom-built microscope. A continuous flow of fresh carbogenated Tyrode's solution at 22 °C was maintained through the sample during the photothermal stimulation experiment.

Bright field illumination was performed using a white LED (6 W LED dual gooseneck illuminator, AMScope, product no. SKU: LED-6W), while the fluorescence imaging was performed using a 473 nm laser (UltraLasers, product no. CST-L-473-50-OEM) and a green fluorescent protein (GFP) filter (Thorlabs, catalog no. MF525-39). The Ca^{2+} fluorescence and bright field images were acquired using a monochromatic complementary metal oxide semiconductor camera (Basler acA3088-57 μm, Basler) using Pylon Viewer (Basler). Bright field images were acquired before laser illumination, and the sequence of Ca^{2+} fluorescence images was acquired at five frames per second during laser illumination. The laser pulses from a 635 nm laser were controlled by TTL signal and applied on the flake–cell interface through a 40×/0.80 NA water immersion objective. ImageJ (Java-based open-source image processing software, NIH) and MATLAB were used for fluorescence intensity analysis. Data are presented as $(F - F_0)/F_0$ *vs* time, where F_0 is the average intensity of the first five seconds before applying the laser pulse, and F is the time-dependent fluorescence intensity. Photothermal stimulation of the film– and dispersed flake–cell interface was performed on 13 and 3 DRG neuron networks, respectively.

ASSOCIATED CONTENT

Supporting Information

The Supporting Information is available free of charge at https://pubs.acs.org/doi/10.1021/acsnano.1c04431.

Movies S1: Ca^{2+} influx achieved by DRG–$Ti_3C_2T_x$ film interfaces (MP4)

Movie S2: Ca^{2+} influx achieved by DRG–$Ti_3C_2T_x$ film interfaces (MP4)

Movie S3: Ca^{2+} influx achieved by DRG–$Ti_3C_2T_x$ flake interface (MP4)

Figures of micropipette calibration, photothermal response of $Ti_3C_2T_x$ flakes under varying laser wavelengths, characterization of $Ti_3C_2T_x$ films, photothermal response of $Ti_3C_2T_x$ films, photothermal stimulation microscope setup, stability evaluation of $Ti_3C_2T_x$ film in physiological conditions, orthogonal sections of DRG–$Ti_3C_2T_x$ flake interface at different z-axis positions, Ca^{2+} influx achieved by DRG–$Ti_3C_2T_x$ film interface, off-cell stimulation of DRG–$Ti_3C_2T_x$ film interface, off-cell and off-$Ti_3C_2T_x$ stimulation of DRG–$Ti_3C_2T_x$ flake interface; tables of AFM results, Raman spectra results, photothermal response of $Ti_3C_2T_x$ flakes (635 and 808 nm illumination), photothermal response of $Ti_3C_2T_x$ films (635 nm illumination), laser conditions on DRG–$Ti_3C_2T_x$ film interface and DRG–$Ti_3C_2T_x$ flake interface to stimulate DRG neurons, comparison of temperature rise of reported photothermal agents, comparison of DRG neuron stimulation energy densities of reported photothermal agents (PDF)

AUTHOR INFORMATION

Corresponding Author

Tzahi Cohen-Karni – *Department of Materials Science and Engineering and Department of Biomedical Engineering, Carnegie Mellon University, Pittsburgh, Pennsylvania 15213, United States;* orcid.org/0000-0001-5742-1007; Email: tzahi@andrew.cmu.edu

Authors

Yingqiao Wang – *Department of Materials Science and Engineering, Carnegie Mellon University, Pittsburgh, Pennsylvania 15213, United States*

Raghav Garg – *Department of Materials Science and Engineering, Carnegie Mellon University, Pittsburgh, Pennsylvania 15213, United States;* orcid.org/0000-0002-3501-6892

Jane E. Hartung – *Department of Neurobiology, University of Pittsburgh, Pittsburgh, Pennsylvania 15213, United States*

Adam Goad – *A.J. Drexel Nanomaterials Institute and Department of Materials Science and Engineering, Drexel University, Philadelphia, Pennsylvania 19104, United States;* orcid.org/0000-0002-5390-6311

Dipna A. Patel – *A.J. Drexel Nanomaterials Institute and Department of Materials Science and Engineering, Drexel University, Philadelphia, Pennsylvania 19104, United States*

Flavia Vitale – *Department of Neurology, Department of Bioengineering, Department of Physical Medicine & Rehabilitation, and Center for Neuroengineering and Therapeutics, University of Pennsylvania, Philadelphia, Pennsylvania 19104, United States; Center for Neurotrauma, Neurodegeneration, and Restoration, Corporal Michael J. Crescenz Veterans Affairs Medical Center, Philadelphia, Pennsylvania 19104, United States*

Michael S. Gold – *Department of Neurobiology, University of Pittsburgh, Pittsburgh, Pennsylvania 15213, United States*

Yury Gogotsi – *A.J. Drexel Nanomaterials Institute and Department of Materials Science and Engineering, Drexel University, Philadelphia, Pennsylvania 19104, United States;* orcid.org/0000-0001-9423-4032

Complete contact information is available at: https://pubs.acs.org/10.1021/acsnano.1c04431

Author Contributions

T.C.-K. designed the research; Y.W., R.G., J.E.H., A.G., and D.A.P. performed the experiments; all authors analyzed the data and discussed the results; and Y.W., R.G., and T.C.-K. wrote the manuscript.

Notes

The authors declare no competing financial interest.

ACKNOWLEDGMENTS

T.C.-K. acknowledges funding support from the National Science Foundation [Award No. CBET1552833], the Defense Advanced Research Projects Agency [Award No. AWD00001593 (416052-5)], and the National Institutes of Health [Award No. R21EB029164]. Y.G acknowledges funding support from the National Science Foundation [Award No. DMR-1740795]. F.V. acknowledges funding support from the National Institutes of Health [Award No. K12HD073945]. We also acknowledge support from the Department of Materials Science and Engineering Materials Characterization Facility supported by Grant MCF-677785.

REFERENCES

(1) Pisanello, F.; Sileo, L.; De Vittorio, M. Micro- and Nanotechnologies for Optical Neural Interfaces. *Front. Neurosci.* **2016**, *10*, 70.

(2) Zimmerman, J. F.; Tian, B. Nongenetic Optical Methods for Measuring and Modulating Neuronal Response. *ACS Nano* **2018**, *12* (5), 4086−4095.

(3) Musk, E. An Integrated Brain-Machine Interface Platform with Thousands of Channels. *Journal of Medical Internet Research* **2019**, *21* (10), No. e16194.

(4) Rivnay, J.; Wang, H.; Fenno, L.; Deisseroth, K.; Malliaras, G. G. Next-Generation Probes, Particles, and Proteins for Neural Interfacing. *Science Advances* **2017**, *3* (6), No. e1601649.

(5) Rastogi, S. K.; Garg, R.; Scopelliti, M. G.; Pinto, B. I.; Hartung, J. E.; Kim, S.; Murphey, C. G.; Johnson, N.; San Roman, D.; Bezanilla, F. Remote Nongenetic Optical Modulation of Neuronal Activity Using Fuzzy Graphene. *Proc. Natl. Acad. Sci. U. S. A.* **2020**, *117* (24), 13339−13349.

(6) Deisseroth, K. Optogenetics. *Nat. Methods* **2011**, *8* (1), 26−29.

(7) Shapiro, M. G.; Homma, K.; Villarreal, S.; Richter, C.-P.; Bezanilla, F. Infrared Light Excites Cells by Changing Their Electrical Capacitance. *Nat. Commun.* **2012**, *3* (1), 1−11.

(8) Wells, J. D.; Kao, C.; Jansen, E. D.; Konrad, P. E.; Mahadevan-Jansen, A. Application of Infrared Light for *in Vivo* Neural Stimulation. *J. Biomed. Opt.* **2005**, *10* (6), No. 064003.

(9) Carvalho-de-Souza, J. L.; Pinto, B. I.; Pepperberg, D. R.; Bezanilla, F. Optocapacitive Generation of Action Potentials by Microsecond Laser Pulses of Nanojoule Energy. *Biophys. J.* **2018**, *114* (2), 283−288.

(10) Carvalho-de-Souza, J. L.; Treger, J. S.; Dang, B.; Kent, S. B.; Pepperberg, D. R.; Bezanilla, F. Photosensitivity of Neurons Enabled by Cell-Targeted Gold Nanoparticles. *Neuron* **2015**, *86* (1), 207−217.

(11) Jiang, Y.; Carvalho-de-Souza, J. L.; Wong, R. C.; Luo, Z.; Isheim, D.; Zuo, X.; Nicholls, A. W.; Jung, I. W.; Yue, J.; Liu, D.-J. Heterogeneous Silicon Mesostructures for Lipid-Supported Bioelectric Interfaces. *Nat. Mater.* **2016**, *15* (9), 1023−1030.

(12) Jiang, Y.; Li, X.; Liu, B.; Yi, J.; Fang, Y.; Shi, F.; Gao, X.; Sudzilovsky, E.; Parameswaran, R.; Koehler, K. Rational Design of Silicon Structures for Optically Controlled Multiscale Biointerfaces. *Nature Biomedical Engineering* **2018**, *2* (7), 508−521.

(13) Fang, Y.; Jiang, Y.; Acaron Ledesma, H.; Yi, J.; Gao, X.; Weiss, D. E.; Shi, F.; Tian, B. Texturing Silicon Nanowires for Highly Localized Optical Modulation of Cellular Dynamics. *Nano Lett.* **2018**, *18* (7), 4487−4492.

(14) VahidMohammadi, A.; Rosen, J.; Gogotsi, Y. The World of Two-Dimensional Carbides and Nitrides (MXenes). *Science* **2021**, *372* (6547), eabf1581.

(15) Rasool, K.; Pandey, R. P.; Rasheed, P. A.; Buczek, S.; Gogotsi, Y.; Mahmoud, K. A. Water Treatment and Environmental Remediation Applications of Two-Dimensional Metal Carbides (MXenes). *Mater. Today* **2019**, *30*, 80−102.

(16) Driscoll, N.; Richardson, A. G.; Maleski, K.; Anasori, B.; Adewole, O.; Lelyukh, P.; Escobedo, L.; Cullen, D. K.; Lucas, T. H.; Gogotsi, Y. Two-Dimensional Ti_3C_2 MXene for High-Resolution Neural Interfaces. *ACS Nano* **2018**, *12* (10), 10419−10429.

(17) Cai, G.; Ciou, J.-H.; Liu, Y.; Jiang, Y.; Lee, P. S. Leaf-Inspired Multiresponsive MXene-Based Actuator for Programmable Smart Devices. *Science Advances* **2019**, *5* (7), No. eaaw7956.

(18) Jhon, Y. I.; Koo, J.; Anasori, B.; Seo, M.; Lee, J. H.; Gogotsi, Y.; Jhon, Y. M. Metallic MXene Saturable Absorber for Femtosecond Mode-Locked Lasers. *Adv. Mater.* **2017**, *29* (40), 1702496.

(19) Lin, H.; Wang, X.; Yu, L.; Chen, Y.; Shi, J. Two-Dimensional Ultrathin MXene Ceramic Nanosheets for Photothermal Conversion. *Nano Lett.* **2017**, *17* (1), 384−391.

(20) Dai, C.; Lin, H.; Xu, G.; Liu, Z.; Wu, R.; Chen, Y. Biocompatible 2D Titanium Carbide (MXenes) Composite Nanosheets for pH-Responsive MRI-Guided Tumor Hyperthermia. *Chem. Mater.* **2017**, *29* (20), 8637−8652.

(21) Naguib, M.; Kurtoglu, M.; Presser, V.; Lu, J.; Niu, J.; Heon, M.; Hultman, L.; Gogotsi, Y.; Barsoum, M. W. Two-Dimensional Nanocrystals Produced by Exfoliation of Ti_3AlC_2. *Adv. Mater.* **2011**, *23* (37), 4248−4253.

(22) Li, R.; Zhang, L.; Shi, L.; Wang, P. MXene Ti_3C_2: An Effective 2D Light-To-Heat Conversion Material. *ACS Nano* **2017**, *11* (4), 3752−3759.

(23) Han, X.; Huang, J.; Lin, H.; Wang, Z.; Li, P.; Chen, Y. 2D Ultrathin MXene-Based Drug-Delivery Nanoplatform for Synergistic Photothermal Ablation and Chemotherapy of Cancer. *Adv. Healthcare Mater.* **2018**, *7* (9), 1701394.

(24) Shuck, C. E.; Sarycheva, A.; Anayee, M.; Levitt, A.; Zhu, Y.; Uzun, S.; Balitskiy, V.; Zahorodna, V.; Gogotsi, O.; Gogotsi, Y. Scalable Synthesis of $Ti_3C_2T_x$ MXene. *Adv. Eng. Mater.* **2020**, *22* (3), 1901241.

(25) Naguib, M.; Unocic, R. R.; Armstrong, B. L.; Nanda, J. Large-Scale Delamination of Multi-Layers Transition Metal Carbides and Carbonitrides "MXenes. *Dalton Transactions* **2015**, *44* (20), 9353−9358.

(26) Mathis, T. S.; Maleski, K.; Goad, A.; Sarycheva, A.; Anayee, M.; Foucher, A. C.; Hantanasirisakul, K.; Shuck, C. E.; Stach, E. A.; Gogotsi, Y. Modified MAX Phase Synthesis for Environmentally Stable and Highly Conductive Ti_3C_2 MXene. *ACS Nano* **2021**, *15* (4), 6420−6429.

(27) Lipatov, A.; Alhabeb, M.; Lukatskaya, M. R.; Boson, A.; Gogotsi, Y.; Sinitskii, A. Effect of Synthesis on Quality, Electronic Properties and Environmental Stability of Individual Monolayer Ti_3C_2 MXene Flakes. *Advanced Electronic Materials* **2016**, *2* (12), 1600255.

(28) Hu, T.; Wang, J.; Zhang, H.; Li, Z.; Hu, M.; Wang, X. Vibrational Properties of Ti_3C_2 and $Ti_3C_2T_2$ (T= O, F, OH) Monosheets by First-Principles Calculations: A Comparative Study. *Phys. Chem. Chem. Phys.* **2015**, *17* (15), 9997−10003.

(29) Sarycheva, A.; Gogotsi, Y. Raman Spectroscopy Analysis of the Structure and Surface Chemistry of $Ti_3C_2T_x$ MXene. *Chem. Mater.* **2020**, *32* (8), 3480−3488.

(30) Sarycheva, A.; Makaryan, T.; Maleski, K.; Satheeshkumar, E.; Melikyan, A.; Minassian, H.; Yoshimura, M.; Gogotsi, Y. Two-Dimensional Titanium Carbide (MXene) as Surface-Enhanced Raman Scattering Substrate. *J. Phys. Chem. C* **2017**, *121* (36), 19983−19988.

(31) Dillon, A. D.; Ghidiu, M. J.; Krick, A. L.; Griggs, J.; May, S. J.; Gogotsi, Y.; Barsoum, M. W.; Fafarman, A. T. Highly Conductive Optical Quality Solution-Processed Films of 2D Titanium Carbide. *Adv. Funct. Mater.* **2016**, *26* (23), 4162−4168.

(32) Jiang, X.; Kuklin, A. V.; Baev, A.; Ge, Y.; Ågren, H.; Zhang, H.; Prasad, P. N. Two-Dimensional MXenes: From Morphological to Optical, Electric, and Magnetic Properties and Applications. *Phys. Rep.* **2020**, *848*, 1−58.

(33) El-Demellawi, J. K.; Lopatin, S.; Yin, J.; Mohammed, O. F.; Alshareef, H. N. Tunable Multipolar Surface Plasmons in 2D $Ti_3C_2T_x$ MXene Flakes. *ACS Nano* **2018**, *12* (8), 8485−8493.

(34) Eom, K.; Im, C.; Hwang, S.; Eom, S.; Kim, T.-S.; Jeong, H. S.; Kim, K. H.; Byun, K. M.; Jun, S. B.; Kim, S. J. Synergistic Combination of Near-Infrared Irradiation and Targeted Gold Nanoheaters for Enhanced Photothermal Neural Stimulation. *Biomed. Opt. Express* **2016**, *7* (4), 1614−1625.

(35) Jiang, Y.; Parameswaran, R.; Li, X.; Carvalho-de-Souza, J. L.; Gao, X.; Meng, L.; Bezanilla, F.; Shepherd, G. M.; Tian, B. Nongenetic Optical Neuromodulation with Silicon-Based Materials. *Nat. Protoc.* **2019**, *14* (5), 1339.

(36) Maleski, K.; Shuck, C. E.; Fafarman, A. T.; Gogotsi, Y. The Broad Chromatic Range of Two-Dimensional Transition Metal Carbides. *Adv. Opt. Mater.* **2021**, *9* (4), 2001563.

(37) Anayee, M.; Kurra, N.; Alhabeb, M.; Seredych, M.; Hedhili, M. N.; Emwas, A.-H.; Alshareef, H. N.; Anasori, B.; Gogotsi, Y. Role of Acid Mixtures Etching on the Surface Chemistry and Sodium Ion Storage in $Ti_3C_2T_x$ MXene. *Chem. Commun.* **2020**, *56* (45), 6090−6093.

https://doi.org/10.1021/acsnano.1c04431
ACS Nano 2021, 15, 14662−14671

(38) Smith, A. M.; Mancini, M. C.; Nie, S. Second Window for *in Vivo* Imaging. *Nat. Nanotechnol.* **2009**, *4* (11), 710−711.
(39) Yong, J.; Needham, K.; Brown, W. G.; Nayagam, B. A.; McArthur, S. L.; Yu, A.; Stoddart, P. R. Gold-Nanorod-Assisted Near-Infrared Stimulation of Primary Auditory Neurons. *Adv. Healthcare Mater.* **2014**, *3* (11), 1862−1868.
(40) Grienberger, C.; Konnerth, A. Imaging Calcium in Neurons. *Neuron* **2012**, *73* (5), 862−885.
(41) Giacobassi, M. J.; Leavitt, L. S.; Raghuraman, S.; Alluri, R.; Chase, K.; Finol-Urdaneta, R. K.; Terlau, H.; Teichert, R. W.; Olivera, B. M. An Integrative Approach to the Facile Functional Classification of Dorsal Root Ganglion Neuronal Subclasses. *Proc. Natl. Acad. Sci. U. S. A.* **2020**, *117* (10), 5494−5501.
(42) Lu, S. G.; Zhang, X.; Gold, M. S. Intracellular Calcium Regulation Among Subpopulations of Rat Dorsal Root Ganglion Neurons. *J. Physiol.* **2006**, *577* (1), 169−190.
(43) Scemes, E.; Giaume, C. Astrocyte Calcium Waves: What They Are and What They Do. *Glia* **2006**, *54* (7), 716−725.
(44) Plaksin, M.; Shapira, E.; Kimmel, E.; Shoham, S. Thermal Transients Excite Neurons through Universal Intramembrane Mechanoelectrical Effects. *Phys. Rev. X* **2018**, *8* (1), No. 011043.
(45) Parameswaran, R.; Carvalho-de-Souza, J. L.; Jiang, Y.; Burke, M. J.; Zimmerman, J. F.; Koehler, K.; Phillips, A. W.; Yi, J.; Adams, E. J.; Bezanilla, F. Photoelectrochemical Modulation of Neuronal Activity with Free-Standing Coaxial Silicon Nanowires. *Nat. Nanotechnol.* **2018**, *13* (3), 260−266.
(46) Lee, A.; Hudson, A.; Shiwarski, D.; Tashman, J.; Hinton, T.; Yerneni, S.; Bliley, J.; Campbell, P.; Feinberg, A. 3D Bioprinting of Collagen to Rebuild Components of the Human Heart. *Science* **2019**, *365* (6452), 482−487.
(47) Wang, K.; Frewin, C. L.; Esrafilzadeh, D.; Yu, C.; Wang, C.; Pancrazio, J. J.; Romero-Ortega, M.; Jalili, R.; Wallace, G. High-Performance Graphene-Fiber-Based Neural Recording Microelectrodes. *Adv. Mater.* **2019**, *31* (15), 1805867.
(48) Quigley, A. F.; Razal, J. M.; Thompson, B. C.; Moulton, S. E.; Kita, M.; Kennedy, E. L.; Clark, G. M.; Wallace, G. G.; Kapsa, R. M. A Conducting-Polymer Platform with Biodegradable Fibers for Stimulation and Guidance of Axonal Growth. *Adv. Mater.* **2009**, *21* (43), 4393−4397.
(49) Swinehart, D. F. The Beer-Lambert Law. *J. Chem. Educ.* **1962**, *39* (7), 333.
(50) Yao, J.; Liu, B.; Qin, F. Rapid Temperature Jump by Infrared Diode Laser Irradiation for Patch-Clamp Studies. *Biophys. J.* **2009**, *96* (9), 3611−3619.

https://doi.org/10.1021/acsnano.1c04431
ACS Nano 2021, 15, 14662−14671